

1 **Scale sensitivity of the Gill circulation, Part I:**

2 **Equatorial case**

3 Beatriz Reboredo

4 *Department of Physics, University of Auckland, Auckland, New Zealand*

5 Gilles Bellon\*

6 *Department of Physics, University of Auckland, Auckland, New Zealand*

7 \*Corresponding author address: Department of Physics, University of Auckland, Auckland, New  
8 Zealand.

9 E-mail: gilles.bellon@auckland.ac.nz

## ABSTRACT

10 We investigate the steady dynamical response of the atmosphere on the  
11 equatorial  $\beta$ -plane to a steady, localized, mid-tropospheric heating source at  
12 the equator. Expanding Gill (1980)'s seminal work, we vary the latitudinal  
13 and longitudinal scales of the diabatic heating pattern while keeping its total  
14 amount fixed. We focus on characteristics of the response which would be  
15 particularly important if the circulation interacted with the hydrologic and en-  
16 ergy cycles: the overturning circulation and the low-level wind. In the limit  
17 of very small scale in either the longitudinal or latitudinal direction, the ver-  
18 tical energy transport balances the diabatic heating and this sets the intensity  
19 of the overturning circulation. In this limit, a fast low-level westerly jet is  
20 located around the center of diabatic heating. With increasing longitudinal or  
21 latitudinal scale of the diabatic heating, the intensity of the overturning cir-  
22 culation decreases and the low-level westerly jet decreases in maximum velocity  
23 and spatial extent relative to the spatial extent of this heating. The associated  
24 low-level eastward mass transport decreases only with increasing longitudinal  
25 scale. These results suggest that moisture-convergence feedbacks will favor  
26 small-scale equatorial convective disturbances while surface-heat-flux feed-  
27 backs would favor small-scale disturbances in mean westerlies and large-scale  
28 disturbances in mean easterlies. Part II investigates the case of off-equatorial  
29 heating.

## 30 **1. Introduction**

31 Gill (1980, hereafter G80)'s seminal work aimed to provide a very simple model of the Walker  
32 circulation that results from the longitudinal distribution of diabatic heating in the tropics, with  
33 maxima of convective heating over the three equatorial land masses or archipelagos – Amazonia,  
34 Africa and the Maritime Continent (Krueger and Winston 1974) – as well as monsoon circula-  
35 tions resulting from off-equatorial regional diabatic heating. G80 showed that the damped, linear,  
36 baroclinic dynamical response of the tropical atmosphere to a localized, steady, mid-tropospheric  
37 diabatic heating reproduces the main features of these circulations.

38 This simple model has become one of the main frameworks to understand tropical circulations  
39 and its solutions are now commonly called Gill circulation. A generalisation of G80's work at-  
40 tempted to simulate the seasonal mean flow realistically (Zhang and Krishnamurti 1996), with  
41 some success. The relevance of G80's work to the atmospheric circulation associated with El Niño  
42 Southern Oscillation was also revealed soon after the publication of the original article (Pazan and  
43 Meyers 1982; Philander 1983). Later studies of the dynamical pattern associated with the Madden-  
44 Julian Oscillation (MJO) (Madden and Julian 1971; Zhang 2005) revealed that this pattern is es-  
45 sentially G80's equatorially symmetric solution (Hendon and Salby 1994; Kiladis et al. 2005).  
46 Very recently, this framework has shown promise to understand the observed pattern of tropical  
47 precipitation in detail (Adam 2018) and the superrotation on tide-locked exoplanets (Showman and  
48 Polvani 2010, 2011; Pierrehumbert and Hammond 2019). Because of this widespread relevance,  
49 G80's model has come to be considered foundational, and is used as a test for further theoretical  
50 development (e.g., Bretherton and Sobel 2003).

51 One of the main caveat of G80's original model is that it only considers mid-tropospheric dia-  
52 batic heating, typically released by condensation associated with deep convection. An alternative

53 framework considers surface sensible heating that ties surface air temperatures to sea surface tem-  
54 peratures, and the corresponding model has shown a dominant role of the surface in driving the  
55 pattern of surface convergence, particularly in the tropical Eastern Pacific (Back and Bretherton  
56 2009), hence making G80’s model less relevant to the Walker circulation than initially concluded.  
57 Nevertheless, as pointed by Neelin (1989), G80’s model can be interpreted as a surface-forcing  
58 model and the two models differ only by the thermodynamic normalization scales and parameters.  
59 The pattern and sensitivities of the Gill circulation are therefore also relevant to the surface-forcing  
60 model.

61 G80 mostly focused on two cases, with latitudinal distributions of diabatic heating for which  
62 there are simple analytical solutions: one symmetric about the equator, the other antisymmetric.  
63 G80 and Heckley and Gill (1984) presented a few additional cases with little analysis. But, obser-  
64 vations document diabatic heating patterns with a wide range of horizontal scales and latitudinal  
65 locations and we have yet to understand the sensitivity of the Gill circulation to these parameters.  
66 The present work aims to understand how the equatorially symmetric Gill circulation depends on  
67 the latitudinal and longitudinal scales of the imposed diabatic heating, with a particular focus on  
68 characteristics of the circulation that, in the real world, interact with the energy cycle: the ver-  
69 tical, overturning circulation which is associated with moisture transport and latent heat release,  
70 and the surface wind which modulates the surface turbulent heat fluxes. Part II investigates the  
71 off-equatorial case (Bellon and Reboredo 2021).

72 In Section 2, we present the solutions to the Matsuno-Gill equations (Matsuno 1966, G80), as  
73 well as the  $f$ -plane case. Section 3 presents some solutions as well as the scale sensitivity of the  
74 overturning circulation and low-level wind. Section 4 summarizes our findings and concludes. For  
75 brevity, we will refer to ”imposed diabatic heating” simply as ”heating” in the next sections.

## 76 2. Method

77 In this section, we summarize the Matsuno-Gill equations and the method of solution by decom-  
78 position in parabolic cylinder functions. We present semi-analytical solutions for a more general  
79 case than in G80, i.e., applicable to heating of varied horizontal extents and we also derive the  
80 asymptotes for small zonal extent of the heating.

### 81 *a. The Matsuno-Gill equations*

82 The Matsuno-Gill equations describe the steady first-baroclinic dynamical response of the trop-  
83 ical atmosphere to prescribed mid-tropospheric heating. They are equivalent to the steady-state,  
84 linear, shallow-water equations with damping terms in the zonal-momentum and continuity equa-  
85 tions. The linear approximation and the neglect of the momentum damping in the meridional  
86 direction (the so-called "longwave approximation") are evaluated in the supplementary material  
87 using simplified versions of the Quasi-equilibrium Tropical Circulation Models (QTCM) (Neelin  
88 and Zeng 2000; Zeng et al. 2000; Lintner et al. 2012) and they are deemed acceptable for large-  
89 scale circulations and realistic amplitudes of heating. Using mid-tropospheric temperature in the  
90 continuity equation instead of pressure (as in G80) or depth of the layer (as in the shallow-water  
91 equations), the Matsuno-Gill equations write:

$$\varepsilon u - \frac{1}{2} y v = -\partial_x T, \quad (1)$$

$$\frac{1}{2} y u = -\partial_y T, \quad (2)$$

$$\varepsilon T + \partial_x u + \partial_y v = Q, \quad (3)$$

92 with  $(u, v)$  the horizontal baroclinic velocity (i.e., the difference between upper-tropospheric and  
 93 lower tropospheric velocity),  $T$  the mid-tropospheric temperature, and  $Q$  the heating. All variables  
 94 are non-dimensional; in particular, distances are normalized by the equatorial radius of deforma-  
 95 tion, which is about 1000 km. These equations are equivalent to Equations (2.6), (2.8), and (2.12)  
 96 in G80. The Matsuno-Gill equations have proven successful in explaining observed tropical vari-  
 97 ability in large part because the gravity-wave phase speed, which is the normalizing scale for  
 98 velocity, is fairly uniform in the tropics as a result of the fairly uniform gross moist stability (Yu  
 99 et al. 1998). We take the value of the damping rate  $\varepsilon$  from G80:  $\varepsilon = 0.1$ , which corresponds to  
 100 a damping time scale of 2.5 days. This damping rate was at times assessed to be too large (e.g.,  
 101 Battisti et al. 1999) and Stechmann and Ogrosky (2014) suggest that the Walker circulation can be  
 102 modeled with no damping at all, if only the longitudinal anomaly of heating is imposed and the  
 103 meridional wind is known. However, other studies suggest that such a large value is justified, in  
 104 particular because of convective momentum transport (Lin et al. 2005, 2008; Iipponen and Donner  
 105 2021). The sensitivity of the Gill circulation to  $\varepsilon$  is related to that of the zonal scale  $L_x$ , as we  
 106 show in Section 2.d.

107 The non-dimensional upward mid-tropospheric vertical velocity is equal to the non-dimensional  
 108 baroclinic divergence and can be written:

$$w = \partial_x u + \partial_y v = Q - \varepsilon T. \quad (4)$$

109 If the damping term  $-\varepsilon T$  is interpreted as a local, diabatic, thermodynamic response to the im-  
 110 posed heating  $Q$ , this equation expresses a balance between vertical advection and diabatic heat-  
 111 ing known as weak-temperature-gradient approximation (Sobel and Bretherton 2000), although  
 112 Bretherton and Sobel (2003) interpreted the damping term differently.

113 G80's framework assumes that the atmospheric response to the heating has a smaller scale than  
 114 the planetary scale so that longitudinal and latitudinal boundaries can be considered infinite. The  
 115 QTCM experiments in the supplementary material, which use realistic boundary conditions, show  
 116 that this assumption is suitable for realistic horizontal extents of the heating on the Earth. This  
 117 might not hold for larger extents or on exoplanets.

118 *b. Solutions to cylinder-mode forcing*

119 G80 presented some analytical solutions to Equations (1)-(3) for heating patterns that follow:

$$Q^{(n)} = F(x)D_n(y) \text{ with } n \in \mathbb{N}, \quad (5)$$

120 and  $F$  a half-period of cosine function in a limited range of longitude:

$$F(x) = \begin{cases} k \cos(kx) & \text{for } |x| < L_x, \\ 0 & \text{for } |x| > L_x, \end{cases} \text{ with } k = \frac{\pi}{2L_x}, \quad (6)$$

121 and  $D_n$  a parabolic cylinder function of degree  $n$ , i.e., the product of a polynomial of degree  $n$  and  
 122 an exponential that limits the latitudinal extent of significant heating:

$$\begin{aligned} D_0 &= \exp\left(-\frac{y^2}{4}\right), \\ D_1 &= y \exp\left(-\frac{y^2}{4}\right), \\ D_{n+1} &= yD_n - nD_{n-1}, \quad \forall n > 0. \end{aligned} \quad (7)$$

123 We will also use  $D_{-1} = D_{-2} = 0$  to write generalized equations. Appendix A documents some of  
 124 the properties of these parabolic cylinder functions that we will also call latitudinal modes. Note

125 that our function  $F$  differs from the function  $F$  in G80 by a factor  $k$  which we introduced to make  
 126 the integral of  $F$  over the longitude independent of  $L_x$ .

127 The method of solution as described in G80 introduces two new variables  $q$  and  $r$  that combine  
 128  $T$  and  $u$  in Equations (1)-(3) as:

$$q = T + u, \quad (8)$$

$$r = T - u. \quad (9)$$

129 For each forcing  $Q^{(n)} = F(x)D_n(y)$  following a latitudinal mode, the solutions  $(q^{(n)}, v^{(n)}, r^{(n)})$  can  
 130 be written as the sum of two additive components (Gill 1980; Heckley and Gill 1984; Abramowitz  
 131 and Stegun 1964),  $(q^{(n,1)}, v^{(n,1)}, r^{(n,1)})$  and  $(q^{(n,2)}, v^{(n,2)}, r^{(n,2)})$ , in which  $q^{(n,1)}$  is proportional to  
 132  $D_n(y)$  and  $q^{(n,2)} \propto D_{n+2}(y)$ ,  $v^{(n,1)} \propto D_{n-1}(y)$  and  $v^{(n,2)} \propto D_{n+1}(y)$ ,  $r^{(n,1)} \propto D_{n-2}(y)$  and  $r^{(n,2)} \propto$   
 133  $D_n(y)$ :

$$\begin{aligned} q^{(n)} &= q^{(n,1)} + q^{(n,2)} = q_n^{(n)}(x)D_n(y) + q_{n+2}^{(n)}(x)D_{n+2}(y), \\ v^{(n)} &= v^{(n,1)} + v^{(n,2)} = v_{n-1}^{(n)}(x)D_{n-1}(y) + v_{n+1}^{(n)}(x)D_{n+1}(y), \\ r^{(n)} &= r^{(n,1)} + r^{(n,2)} = r_{n-2}^{(n)}(x)D_{n-2}(y) + r_n^{(n)}(x)D_n(y). \end{aligned} \quad (10)$$

134 The functions of longitude  $x$  in the first component are solutions of:

$$\frac{dq_n^{(n)}}{dx} - (2n-1)\epsilon q_n^{(n)} = -(n-1)F(x), \quad (11)$$

$$v_{n-1}^{(n)} = 2n\epsilon q_n^{(n)} - nF(x), \quad (12)$$

$$r_{n-2}^{(n)} = nq_n^{(n)}. \quad (13)$$

135 And in the second component, they are solutions of:

$$\frac{dq_{n+2}^{(n)}}{dx} - (2n+3)\varepsilon q_{n+2}^{(n)} = -F(x), \quad (14)$$

$$v_{n+1}^{(n)} = 2(n+2)\varepsilon q_{n+2}^{(n)} - F(x), \quad (15)$$

$$r_n^{(n)} = (n+2)q_{n+2}^{(n)}. \quad (16)$$

136 Solving Equations (11) and (14) for  $q_n^{(n)}$  and  $q_{n+2}^{(n)}$  yields the complete solution  $q^{(n)}$  since Equations  
 137 (12), (13), (15) and (16) give  $v_{n-1}^{(n)}$ ,  $v_{n+1}^{(n)}$ ,  $r_{n-2}^{(n)}$ , and  $r_n^{(n)}$  as functions of  $q_n^{(n)}$  and  $q_{n+2}^{(n)}$ . The solutions  
 138 detailed in G80 are for  $n = 0$  (symmetric heating) and  $n = 1$  (antisymmetric heating).

139 For  $n = 0$ , the longitudinal dependence of the first component can be written:

$$\{\varepsilon^2 + k^2\}q_0^{(0)} = \begin{cases} 0 & \text{if } x < -L_x, \\ \varepsilon k \cos(kx) + k^2 \sin(kx) + k^2 \exp[-\varepsilon(x + L_x)] & \text{if } |x| < L_x, \\ 2k^2 \cosh(\varepsilon L_x) \exp\{-\varepsilon x\} & \text{if } x > L_x; \end{cases} \quad (17)$$

140 for  $n = 1$ :

$$q_1^{(1)} = 0; \quad (18)$$

141 and for  $n > 1$ :

$$\frac{(2n-1)^2 \varepsilon^2 + k^2}{n-1} q_n^{(n)} = \begin{cases} 2k^2 \cosh[(2n-1)\varepsilon L_x] \exp[(2n-1)\varepsilon x] & \text{if } x < -L_x, \\ (2n-1)\varepsilon k \cos(kx) - k^2 \sin(kx) + k^2 \exp[(2n-1)\varepsilon(x-L_x)] & \text{if } |x| < L_x, \\ 0 & \text{if } x > L_x. \end{cases} \quad (19)$$

142 Note that only  $q_0^{(0)}$  is non-zero east of the heating region ( $x > L_x$ ), and zero west of it ( $x < -L_x$ ).

143 All other components extend west of the heating region.

144 It is clear from the similarity of Equations (11) and (14) and from the same boundary and con-  
 145 tinuity conditions that apply to  $q_n^{(n)}$  and  $q_{n+2}^{(n)}$  that the longitudinal dependence of the second com-  
 146 ponent can be written, for all  $n$ :

$$q_{n+2}^{(n)} = \frac{1}{n+1} q_{n+2}^{(n+2)}. \quad (20)$$

147 To get back to the physical non-dimensional variables, we use  $T^{(n)} = (q^{(n)} + r^{(n)})/2$  and  $u^{(n)} =$   
 148  $(q^{(n)} - r^{(n)})/2$ . The first component of the solution is, for  $n = 0$ :

$$\left. \begin{aligned} u^{(0,1)} &= T^{(0,1)} = \frac{1}{2} q_0^{(0)}(x) D_0(y), \\ v^{(0,1)} &= 0; \end{aligned} \right\} \quad (21)$$

149 for  $n = 1$ :

$$\left. \begin{aligned} u^{(1,1)} &= T_1^{(1,1)} = 0, \\ v^{(1,1)} &= -F(x) D_0(y); \end{aligned} \right\} \quad (22)$$

150 for  $n > 1$ , it is

$$\left. \begin{aligned} T^{(n,1)} &= \frac{1}{2}q_n^{(n)}(x)[D_n(y) + nD_{n-2}(y)], \\ u^{(n,1)} &= \frac{1}{2}q_n^{(n)}(x)[D_n(y) - nD_{n-2}(y)], \\ v^{(n,1)} &= n[2\epsilon q_n^{(n)}(x) - F(x)]D_{n-1}(y); \end{aligned} \right\} \quad (23)$$

151 And the solution for the second component is, for all  $n$ :

$$\left. \begin{aligned} T^{(n,2)} &= \frac{1}{2}q_{n+2}^{(n)}(x)[D_{n+2}(y) + (n+2)D_n(y)], \\ u^{(n,2)} &= \frac{1}{2}q_{n+2}^{(n)}(x)[D_{n+2}(y) - (n+2)D_n(y)], \\ v^{(n,2)} &= [2(n+2)\epsilon q_{n+2}^{(n)}(x) - F(x)]D_{n+1}(y). \end{aligned} \right\} \quad (24)$$

152 Following from Equation (20), it is straightforward that the second component of the temperature  
 153 and zonal wind response to heating along  $D_n$  has the same pattern as the first component of the  
 154 response to heating along  $D_{n+2}$ :  $T^{(n,2)} = T^{(n+2,1)}/(n+1)$  and  $u^{(n,2)} = u^{(n+2,1)}/(n+1)$ .

155 Both components' contributions to the mid-tropospheric vertical velocity can be written:

$$w^{(n,m)} = \frac{1}{2}F(x)D_n(y) - \epsilon T^{(n,m)}, \quad (25)$$

156 for all  $n$  and for  $m = 1$  or  $2$ .

157 Note that:

- 158 1. Only the first component of the solution for  $n = 0$  extends beyond  $x = L_x$  in the longitudinal  
 159 direction. It is associated with no meridional wind and has a Kelvin-wave structure as noted  
 160 in G80.

161 2. All other components have a Rossby-wave structure with gyres meridionally aligned in the  
 162 region  $x < L_x$ , with a westward extent that decreases with  $n$ . On each side of the equator,  
 163 cyclonic and anticyclonic gyres alternate in the poleward direction.

164 *c. More general forcing*

165 Because of the variety of scales of diabatic heating in the tropics, it is of interest to understand  
 166 the dynamical response to heating with a wide range of horizontal extents from the synoptic to  
 167 the planetary scale. The present work expands on the results of G80 by studying the response to  
 168 heating  $Q$  with a similar shape as in G80 (half-period cosine in the longitudinal direction, Gaussian  
 169 in the meridional direction), but with varying longitudinal and latitudinal extents (this Part I), and  
 170 latitude (Part II).

171 Let's start with the same longitudinal distribution as in G80 and a very general latitudinal distri-  
 172 bution:

$$Q = F(x)D(y), \quad (26)$$

173 with  $F(x)$  in the form given by Equation (6), and  $D(y)$  a bounded function of  $y$ .

174 With inner product  $\langle f, g \rangle = \int fg dy$ ,  $D_n$  functions form an orthogonal basis  $(D_n)_{n \in \mathbb{N}}$ . The norm  
 175 of each  $D_n$  is  $\sqrt{n! \sqrt{2\pi}}$ . Any bounded function  $D$  can be decomposed in a series on the basis  
 176  $(D_n)_{n \in \mathbb{N}}$ :

$$D(y) = \sum_{n=0}^{\infty} a_n(L_y) D_n(y). \quad (27)$$

177 It follows that  $Q$  can also be written as a series of  $Q_{n \in \mathbb{N}}^{(n)}$ :

$$Q = \sum_{n=0}^{\infty} a_n Q^{(n)} F(x). \quad (28)$$

178 Because the Matsuno-Gill equations are linear, the solution to the steady, linear equation set  
 179 (1)-(3) forced by  $Q = F(x)D(y)$  can be determined semi-analytically as a series of the solutions to  
 180 heating patterns with latitudinal distributions  $D_n$ :

$$\begin{aligned}
 T &= \sum_{n=0}^{\infty} a_n T^{(n)}, \\
 u &= \sum_{n=0}^{\infty} a_n u^{(n)}, \\
 v &= \sum_{n=0}^{\infty} a_n v^{(n)}.
 \end{aligned}
 \tag{29}$$

181 We will study the cases of a Gaussian latitudinal distribution of  $Q$  of varying latitudinal extent  
 182 centered on latitude  $y_0$ :

$$D(y) = \frac{1}{L_y} \exp\left(-\frac{(y-y_0)^2}{4L_y^2}\right).
 \tag{30}$$

183 With such a formulation, the heating  $Q$  is a "patch" of heating centered on  $(x, y) = (0, y_0)$ . This  
 184 patch is close to circular for  $L_x = 3L_y$ . By design, the maximum heating varies with  $L_x$  and  $L_y$  in  
 185  $k/L_y$  so that the total heating provided to the atmosphere is independent of the longitudinal and  
 186 latitudinal scales:

$$[Q] = \int_{-L_x}^{+L_x} \int_{-\infty}^{+\infty} Q dx dy = 4\sqrt{\pi},
 \tag{31}$$

187 with the brackets  $[\cdot]$  indicating global integration. This allows us to isolate the sensitivity to the  
 188 scales independently from that to a change in global energy input.

189 In this Part I, we focus on heating symmetric with respect to the equator, i.e. with  $y_0 = 0$ . The  
 190 coefficients  $a_n$  are:

$$a_{2n} = \frac{1}{2^n n!} \left( \frac{L_y^2 - 1}{L_y^2 + 1} \right)^n \sqrt{\frac{2}{L_y^2 + 1}}, \quad (32)$$

$$a_{2n+1} = 0. \quad (33)$$

191 In practice, since the infinite sum in Equation (27) is convergent, it can be approximated by  
 192 a finite sum up to a value  $m$  following a convergence criterion (Cauchy 1821). The conver-  
 193 gence criterion requires to set a positive error of tolerance  $\eta$  for which any index  $l > m$  satisfies  
 194  $\|\sum_{n=0}^l a_n(L_y)D_n(y) - \sum_{n=0}^{l-1} a_n(L_y)D_n(y)\| \leq \eta$ . This value  $m$  will differ for different values of  $L_y$ .  
 195 For example, setting  $\eta = 0.001$ , one mode is enough for the trivial case where  $L_y = 1$ , whereas  
 196 for  $L_y = 0.5$  we need 10 modes to meet the error criterion, and more modes are needed for smaller  
 197  $L_y$ . Heckley and Gill (1984) used the same approach to study the transient response to a very  
 198 localized heating. The results on the Gill circulation presented in this article are the finite-sum  
 199 approximations of the semi-analytical solutions (Eq. 29), except in the case of the limit  $L_x \rightarrow 0$   
 200 for which we can find analytical expressions.

#### 201 *d. Limits for heating with small longitudinal extent*

202 Here, we explore the asymptotic solutions for  $L_x \rightarrow 0$ , but this is also relevant for the limit  
 203  $\varepsilon \rightarrow 0$ . Indeed, it is easy to write the solutions in Equations (17)-(20) as functions of  $\varepsilon L_x$  and  $x/L_x$   
 204 (using  $k = \pi/(2L_x)$ ), with no other dependency on  $\varepsilon$  or  $L_x$ . This means that the sensitivity of the  
 205 solutions to  $\varepsilon$  is the same as the sensitivity to  $L_x$ , except that the patterns scale zonally with  $L_x$ .  
 206 All the characteristics of the circulation that we study will actually have identical sensitivities to  $\varepsilon$   
 207 and to  $L_x$ .

208 We focus on the interval  $-L_x \leq x \leq L_x$ . Outside this interval, qualitatively, there is subsidence,  
 209 but there is no simple expression for the solutions. Note that this limit is identical to the limit  
 210  $\varepsilon \rightarrow 0$  if we consider the zonal coordinate  $x/L_x$  (see Section 2.a).

211 As pointed in G80, the damping in the meridional-momentum equation is negligible only if  
 212  $\varepsilon k \ll 1$ . In the limit  $L_x \rightarrow 0$ , this is not verified, so the limit of the Gill circulation for  $L_x \rightarrow 0$   
 213 is not well-described by the Matsuno-Gill equations. Nevertheless, the supplementary material  
 214 shows that meridional-momentum damping has a small impact on the Gill circulation down to  
 215  $L_x = 0.075$  (or about 70 km), i.e. down to the smallest synoptic scales. Therefore, for large-  
 216 scale circulations, the asymptote of the solution to the Matsuno-Gill equations for  $L_x \rightarrow 0$  is still  
 217 relevant.

218 In this limit,  $k \rightarrow +\infty$  and we have:

$$\begin{aligned}
 q_0^{(0)} &\sim 1 + \sin kx, \\
 q_n^{(n)} &\sim (n-1)(1 - \sin kx) \text{ for } n > 0, \\
 q_{n+2}^{(n)} &\sim (1 - \sin kx) \text{ for all } n,
 \end{aligned}
 \tag{34}$$

219 for  $|x| \leq L_x$ . Noting that:

$$\begin{aligned}
 D_n + nD_{n-2} &= -\frac{1}{n-1} (D_n - nyD_{n-1}) \text{ for } n > 1 \text{ and} \\
 D_{n+2} + (n+2)D_n &= D_n + yD_{n+1},
 \end{aligned}$$

220 we can write the temperature responses to cylindrical forcing as follows:

$$\begin{aligned}
T^{(0,1)} &\sim \frac{1}{2}(1 + \sin kx) D_0(y), \\
T^{(1,1)} &\sim 0 \\
T^{(n,1)} &\sim -\frac{1}{2}(1 - \sin kx) [D_n(y) - nyD_{n-1}(y)] \text{ for } n > 1, \\
T^{(n,2)} &\sim \frac{1}{2}(1 - \sin kx) [D_n(y) + yD_{n+1}(y)].
\end{aligned} \tag{35}$$

221 By combining the odd- $n$  latitudinal modes using Equation (7), we can further write:

$$T^{(0)} \sim \frac{1}{2}(1 - \sin kx) y^2 D_0(y) + D_0(y), \tag{36}$$

$$T^{(n)} \sim \frac{1}{2}(1 - \sin kx) y^2 D_n(y) \text{ for } n > 0. \tag{37}$$

222 By multiplying  $T^{(n)}$  by  $a_n$  and summing over  $n$ , we get the asymptote of the solution  $T$  for  $L_x \rightarrow 0$ :

$$T \sim \frac{1}{2}(1 - \sin kx) y^2 D(y) + a_0 D_0(y). \tag{38}$$

223 This result is valid for any bounded function  $D$ , not only the Gaussian distribution given in Equ-

224 tion (30). A scale analysis reveals the first order for  $w$ :  $\varepsilon T = \mathcal{O}(D)$ , while  $Q = \mathcal{O}(D/L_x)$  so that

225  $\varepsilon T \ll Q$  and:

$$w \sim k \cos(kx) D(y) = Q, \tag{39}$$

226 which expresses a balance between heating and transport.

227 The asymptotes for the zonal and meridional winds can be obtained using Equations (1) and (2):

$$u \sim -2(1 - \sin kx) \left[ D(y) + \frac{y}{2} \frac{dD}{dy} \right] + a_0 D_0(y), \quad (40)$$

$$v \sim -k \cos(kx) y D(y), \quad (41)$$

228 valid for any bounded function  $D$ . For heating following a Gaussian distribution symmetric about  
 229 the equator (Eq. (30) with  $y_0 = 0$ ), which is the case of interest in this Part I, Equation (40) further  
 230 simplifies into:

$$u \sim -2(1 - \sin kx) \left( 1 - \frac{y^2}{4L_y^2} \right) D(y) + a_0 D_0(y), \quad (42)$$

231 which is negative around the heating center, indicating upper-tropospheric easterlies and low-level  
 232 westerlies in this region. The zonal wind is maximum on the equator at the western boundary of  
 233 the heating region ( $x = -L_x$ ), and it decreases both eastward and poleward, eventually changing  
 234 sign.

235 If  $L_y \rightarrow 0$  as well, all the results above hold, and the last term on the right-hand side of Equation  
 236 (42) is negligible: the equatorial zonal wind scales with  $1/L_y$  and the jets extends in longitude all  
 237 the way to the eastern boundary of the heating region ( $x = L_x$ ) and in latitude to  $y = \pm 2L_y$  on both  
 238 sides of the heating center. This limit shows that the Gill response is zonally asymmetric even  
 239 for scales that are much smaller than the equatorial radius of deformation: it is characterized by a  
 240 westerly low-level jet at the heating center. This suggests significant limitations on the approach  
 241 considering that small systems in the equatorial regions are well approximated by non-rotating  
 242 systems.

243 *e. A baseline: the  $f$ -plane case*

244 The zonal asymmetry which is characteristic of the Gill circulation results from the  $\beta$  effect.  
245 This calls for a further evaluation of this effect. To do so, we also present some elements of the  
246 solution on an  $f$ -plane. In this case, the solution is a damped inertio-gravity wave. Equations for  
247 momentum and continuity reduce to:

$$w = -\frac{\varepsilon}{\varepsilon^2 + f^2} \Delta T, \quad (43)$$

$$T = \frac{1}{\varepsilon} Q + \frac{1}{\varepsilon^2 + f^2} \Delta T, \quad (44)$$

248 in which  $\Delta$  is the Laplacian operator. In the equatorial case,  $f = 0$ , i.e. rotation is neglected, and  
249 the solution is a damped gravity wave, in which the horizontal wind is exclusively divergent.

250 These equations make clear that, in the absence of any circulation, the temperature response  
251 is the direct thermodynamic response  $Q/\varepsilon$ . Vertical energy transport appears as a diffusive term  
252  $\Delta T/(\varepsilon^2 + f^2)$  that damps temperature gradients and makes the equilibrium temperature response  
253 to heating spatially smoother than the heating itself. Both the ascending motion and diffusive  
254 effect are larger in the equatorial case ( $f = 0$ ) than in the off-equatorial case ( $f \neq 0$ ).

255 Scale analysis allows us to establish the limits of this solution for small horizontal extent of  
256 the heating, if  $L_x \rightarrow 0$  (or  $L_y \rightarrow 0$ , since this set of equations is isotropic). If the scaling of the  
257 temperature is  $\mathcal{T}$ , the scaling of the diffusive term on the right hand side of Equation (44) is:

$$\frac{1}{\varepsilon^2 + f^2} \Delta T \sim \frac{1}{\varepsilon^2 + f^2} \frac{\mathcal{T}}{L_x^2} \gg \mathcal{T}, \quad (45)$$

258 Consequently, the term on the left-hand side of Equation (44) is negligible, and this equation shows  
259 a balance between vertical transport and heating  $w \sim Q$  in the limit of very small horizontal extents  
260 of the heating, like in the Gill circulation.

### 261 3. Results

#### 262 a. Temperature and wind response

263 Here, we present the features of the solutions in terms of temperature, surface winds and mid-  
264 tropospheric vertical motion for heating distributions  $Q$  with a few different horizontal extents.  
265 Figure 1 depicts contours of temperature perturbation and surface velocity field for the Gill cir-  
266 culation forced by heating of different meridional scales, but with the same total, horizontally  
267 integrated heating  $[Q]$ :  $L_y = 1$  (equatorial radius of deformation, Fig. 1a),  $L_y = 1/2$  (Fig. 1b), and  
268  $L_y = 1/4$  (Fig. 1c), with a fixed aspect ratio so that  $L_x = 3L_y$  (corresponding to a heating pattern  
269 close to circular). Figure 2 shows the corresponding contours of mid-tropospheric vertical velocity  
270 together with contours of heating. Figures 1a and 2a are almost identical to the symmetric forcing  
271 presented in G80, the only difference being the longitudinal extent:  $L_x = 3$  here while G80 showed  
272 solutions for  $L_x = 2$ .

273 As expected, the Gill circulation exhibits Kelvin-wave easterlies east of the heating region and  
274 cyclonic gyres straddling the equator west of it, with maxima of temperature at the center of the  
275 gyres (Fig. 1). As the horizontal extent of the heating is decreased, winds get stronger, especially  
276 the equatorial westerly jet between the gyres, and the off-equatorial temperature maxima move  
277 closer to the equator, they even merge for small  $L_y$  (Fig. 1). As the horizontal extent of the heating  
278 is decreased, the maximum vertical speed increases faster than the maximum heating, which scales  
279 with  $L_x^{-1}L_y^{-1}$ , and the vertical speed pattern becomes more similar to that of the heating (Fig. 2).

Overall, the meridional extent of the response decreases. The eastward extent of the temperature and horizontal-wind response increases and the westward extent decreases slightly with decreasing horizontal extent of heating (Fig. 1). This reveals a decrease in the Rossby-wave response in the west, while the Kelvin-wave response expands eastward. The latter corresponds to an increase in the projection of  $D$  on  $D_0$  with decreasing  $L_y$ , which is consistent with the expression of  $a_0$  (see Eq. (27)).

### *b. Overturning Circulation*

One of the most important characteristics of a tropical circulation is its overturning mass flux, because of its potential interaction with the hydrologic cycle. We define the intensity of the overturning circulation  $\Gamma$  as the upward vertical mass flux integrated over the horizontal domain (which, by mass conservation, is the same as the downward vertical mass flux integrated over the domain):

$$\Gamma = \iint_{w>0} w dx dy. \quad (46)$$

$\Gamma$  can be computed numerically using the expression of  $w$  in Equation (25).

Figure 3a shows the intensity  $\Gamma$  of the overturning circulation, as a function of the characteristic extents of heating  $L_x$  and  $L_y$ . For  $L_x \rightarrow 0$  or  $L_y \rightarrow 0$ ,  $\Gamma$  has the same limit. As shown in Section 2.d, in the limit  $L_x \rightarrow 0$ ,  $w \sim Q > 0$  in the heating region and by spatial integration,  $\Gamma \sim [Q]$ . It appears that  $\Gamma$  has the same limit for  $L_y \rightarrow 0$ .

The  $f$ -plane case described in Section 2.e sheds some light on this: the damped inertio-gravity wave presents the same limit for  $w \sim Q$  for  $L_x$  or  $L_y \rightarrow 0$ , and therefore also  $\Gamma \sim [Q]$ . For small-scale heating, the heating  $Q$  and the local temperature response to this heating  $Q/\varepsilon$  are very peaked at the center of heating, the diffusive transport is therefore very efficient at reducing the tempera-

300 ture response, so efficient that the resulting temperature perturbation is negligible compared to  $Q$   
301 and the main balance is between vertical energy transport and heating ( $w \sim Q$ ). We hypothesize  
302 that the physical mechanism is the same in the Gill circulation for both  $L_x \rightarrow 0$  and  $L_y \rightarrow 0$ .

303  $\Gamma$  decreases with increasing  $L_x$  and  $L_y$ , in a similar fashion for both scales (for  $L_y = 1$ , the sensi-  
304 tivity to  $L_x$  is also documented in Iipponen and Donner (2021)). There are two factors contributing  
305 to this:

- 306 • First, even without rotation (i.e., the  $f$ -plane case detailed in Section 2.e with  $f = 0$ )  $\Gamma$  de-  
307 creases with increasing horizontal extent of the heating. Indeed, as the horizontal extent in-  
308 creases,  $Q$  becomes spatially smoother because  $[Q]$  is fixed. As a result, the diffusive effect of  
309 large scale transport becomes less efficient at damping the temperature response.  $w = Q - \epsilon T$   
310 becomes smaller, and by spatial integration, this decrease is transmitted to  $\Gamma$ . A similar sen-  
311 sitivity to zonal scale and vertical scales was found by Iipponen and Donner (2021) for a  
312 non-rotating, meridionally averaged model of the Walker circulation.
- 313 • Rotation increases the sensitivity of the overturning circulation to the horizontal extent of the  
314 heating pattern. Indeed, Figure 1 shows that rotation creates gyres straddling the equator,  
315 which are mostly rotational, while the damped gravity wave is exclusively divergent. The  
316 poleward flow associated with these gyres compensates most of their equatorward flow and  
317 we expect the meridional wind to contribute little to the divergence of the horizontal wind  
318 and upward motion. We can also propose an energetic interpretation of this sensitivity<sup>1</sup>. The  
319 energy source of the system is the heating, and the sinks are the kinetic energy loss through  
320 Rayleigh friction and the thermal energy loss through Newtonian cooling, the sum of which  
321 is proportional to the total energy (kinetic plus thermal). Assuming the global thermal energy

---

<sup>1</sup>The supplementary material shows that our quasi-analytical solutions to the linear equations with the longwave approximation are very similar to the numerical solutions to the full non-linear, energy-conserving equations, which shows that our equations approximately satisfy energy conservation and energy-based reasoning is sound.

322 (and thermal energy loss) does not vary significantly with rotation, the global kinetic energy  
 323 should be similar with and without rotation. Without rotation, all kinetic energy corresponds  
 324 to divergent motion while in the rotating case part of it is associated with rotational motion  
 325 and the kinetic energy of divergent motion is smaller than without rotation. We can therefore  
 326 expect the divergent flow to be weaker with rotation than without.

327 A more quantitative understanding of  $\Gamma$  can be hindered by the fact that the domain of integration  
 328 in Equation (46) is determined by the field  $w$  itself, which we know only as a sum. But Figure 2  
 329 suggests that the upward motion is limited to a region between  $-L_x$  and  $L_x$  in longitude, with a  
 330 meridional extent that scales with  $L_y$ . We find that  $\Gamma$  can be approximated by the integral  $\Gamma_*$  of  $w$   
 331 over the domain  $([-L_x, L_x], [-4L_y, 4L_y])$ , with the latitudinal bounds corresponding to twice the  
 332 e-folding distance of  $D$ :

$$\Gamma_* = \int_{-4L_y}^{4L_y} \int_{-L_x}^{L_x} w \, dx \, dy \approx \Gamma. \quad (47)$$

333 Approximating  $\Gamma$  by  $\Gamma_*$  introduces an error that is small ( $< 5\%$ ) for most relevant values of  
 334  $L_x$  and  $L_y$ , but becomes larger as both  $L_x$  and  $L_y$  are large. It is up to 16%, for the maximum  
 335 values we have considered  $(L_x, L_y) = (6, 2)$ ; nevertheless, combinations of such large values of  $L_x$   
 336 and  $L_y$  are outside the observed range ( $L_x = 6$  corresponds to more than a quarter of the Earth's  
 337 circumference and  $L_y = 2$  to heating that extend to the extratropics in both hemispheres), and  $\Gamma_*$   
 338 is therefore a reasonable approximation to  $\Gamma$  for realistic extents of  $Q$ . This approximation allows  
 339 us to decompose the intensity of the overturning circulation into the sum of contributions from the  
 340 different latitudinal modes:

$$\Gamma_* = \sum_{n=0}^{\infty} \Gamma_*^{(2n)} = \sum_{n=0}^{\infty} \Gamma_*^{(2n,1)} + \Gamma_*^{(2n,2)}, \quad (48)$$

341 with  $\Gamma_*^{(2n,1)}$  and  $\Gamma_*^{(2n,2)}$  the contributions of the first and second part of the response to the projec-  
 342 tion of the heating latitudinal distribution  $D$  on the  $n^{\text{th}}$  symmetric latitudinal modes  $D_{2n}$ , i.e.,  $a_{2n}$   
 343 multiplied by the response to heating in the form  $F(x)D_{2n}(y)$ .

$$\Gamma_*^{(2n,i)} = a_{2n} \int_{-4L_y}^{4L_y} \int_{-L_x}^{L_x} w^{(2n,i)} dx dy, \quad (49)$$

344 for  $i = 1, 2$ . Appendix B shows that we can write these contributions as:

$$\Gamma_*^{(2n,1)} = \gamma_{2n}(L_x) f_{2n}(L_y) + [1 - \gamma_{2n}(L_x)] g_{2n,1}(L_y) \quad (50)$$

$$\Gamma_*^{(2n,2)} = \gamma_{2n+2}(L_x) f_{2n}(L_y) + [1 - \gamma_{2n+2}(L_x)] g_{2n,2}(L_y) \quad (51)$$

345 with the variation in  $L_x$  given by the series of functions  $\gamma_{2n}$ :

$$\begin{aligned} \gamma_0 &= \frac{1}{2} q_0^{(0)}(L_x) = \frac{1}{2} \frac{1 + e^{-2\epsilon L_x}}{1 + \epsilon^2 l_x^2}, \\ \gamma_{2n} &= \frac{1}{2} \frac{q_{2n}^{(2n)}(-L_x)}{2n-1} = \frac{1}{2} q_{2n}^{(2n-2)}(-L_x) = \frac{1}{2} \frac{1 + e^{-2(4n-1)\epsilon L_x}}{1 + (4n-1)^2 \epsilon^2 l_x^2} \text{ for } n > 0, \end{aligned} \quad (52)$$

346 with  $l_x = 1/k = 2L_x/\pi$ ; and the variation in  $L_y$  given by:

$$f_{2n} = a_{2n}(L_y) I_{2n} \text{ with } I_{2n} = \int_{-4L_y}^{4L_y} D_{2n} dy, \quad (53)$$

$$g_{2n,1} = -\frac{8n}{4n-1} a_{2n}(L_y) D_{2n-1}(4L_y), \text{ and} \quad (54)$$

$$g_{2n,2} = \frac{4}{4n+3} a_{2n}(L_y) D_{2n+1}(4L_y). \quad (55)$$

347 Figure 4 shows these functions for  $n \leq 5$ . In terms of amplitude,  $\Gamma_*$  is dominated by the response  
 348 of mode  $n = 0$ , because the differences  $f_0 - g_{0,1} = f_0$  and  $f_0 - g_{0,2}$  are the largest, and because

349  $\gamma_0$ 's decrease with increasing  $L_x$  is the slowest of all  $\gamma_{2n}$ . But in terms of sensitivity to  $L_x$  and  $L_y$ ,  
 350 modes with larger  $n$  contribute significantly.

351 Since  $\gamma_{2n}(0) = 1$ ,  $\Gamma_*^{(2n,i)}(0, L_y) = f_{2n}$  for all  $n$  and  $i = 1, 2$ ; we can establish that:

$$\Gamma_*(0, L_y) = 2 \int_{-4L_y}^{4L_y} \sum_{n=0}^{\infty} a_{2n} D_{2n} dy = 2 \int_{-4L_y}^{4L_y} D dy = \text{erf}(2)[Q], \quad (56)$$

352 which is a good approximation to  $\Gamma(0, L_y) = [Q]$  ( $\text{erf}(2) \approx 0.995$ ). This limit is independent of  $L_y$ ,  
 353 which is consistent with Figure 3a.  $\Gamma_*$  also appears to tend towards a value close to  $[Q]$  for  $L_y \rightarrow 0$ .

354 With  $\gamma_{2n} \rightarrow 0$  for  $L_x \rightarrow \infty$ , each contribution  $\Gamma_*^{(2n,i)}$  tends towards  $g_{2n,i}$  for  $L_x \rightarrow \infty$ . Figure 4a  
 355 shows the functions  $\gamma_{2n}$  for  $n$  from 0 to 5. The decrease of  $\gamma_0$  with  $L_x$  results from the sensitivity  
 356 of the diffusive effect of large-scale circulation described above (since the first component of the  
 357 response to  $D$ 's projection onto  $D_0$  is a damped Kelvin wave,  $\Gamma_*^{(0,1)}$  is not affected by rotational  
 358 effects). The decay of  $\gamma_{2n}$  with  $L_x$  is increasingly fast with increasing  $n$ , which means that the  
 359 larger  $n$  (and the larger  $i$ ), the faster the convergence of  $\Gamma_*^{(2n,i)}$  towards its limit  $g_{2n,i}$  for  $L_x \rightarrow \infty$ .  
 360 A more intricate latitudinal structure of heating (i.e., a larger  $n$ ) yields a stronger sensitivity of  
 361 the circulation response to  $L_x$ . We can attribute this change in sensitivity to the effect of rotation:  
 362 for larger  $n$ , the heating pattern has extrema further from the equator, where the effect of rotation  
 363 is larger and temperature anomalies generate circulations that are increasingly rotational and less  
 364 and less convergent, creating less vertical motion.

365 From its value for  $L_x = 0$  independent of  $L_y$  (see Eq. (56)), the decrease of  $\Gamma_*$  with  $L_x$  is  
 366 determined by the circulation responses to heating along  $D_{2n}$ ,  $f_{2n}(L_y)$  for  $L_x = 0$  and  $g_{2n,i}(L_y)$  for  
 367  $L_x \rightarrow \infty$ . The sensitivity of these functions  $f_{2n}$  and  $g_{2n,i}$  to  $L_y$  result from (i) the change in projection  
 368 of  $D$  onto the latitudinal modes  $D_{2n}$ , given by  $a_{2n}$ , and (ii) the extension of the horizontal domain

369 of integration ( $[-L_x, L_x], [-4L_y, 4L_y]$ ) with  $L_y$ . Figures 4b-d show functions  $f_{2n}(L_y)$  and  $g_{2n,i}(L_y)$ .

370 We can distinguish two domains:

371 •  $L_y \geq 1$ : for  $L_y = 1$ ,  $D = D_0$  – this is the case described in G80. For increasing  $L_y > 1$ ,  $D$   
 372 is less and less peaked at the equator; it projects increasingly on higher-and-higher- $n$   $D_n$   
 373 while projecting less and less on  $D_0$ , as shown in Figure 4b. Because of the exponential  
 374 decay of  $D_n(4L_y)$  with increasing  $L_y$ ,  $g_{2n,1}$  and  $g_{2n,2}$  are negligible in this range of  $L_y$  (see  
 375 Fig. 4c,d); for the same reason,  $I_{2n}$  is similar to its limit  $I_{2n}^\infty$ <sup>2</sup> for  $L_y \rightarrow \infty$ . As a result,  
 376  $\Gamma_*^{(2n,i)} \approx \gamma_{2(n+i-1)}(L_x) a_{2n}(L_y) I_{2n}^\infty$  and its variation with  $L_y$  is mostly determined by the  
 377 variation of  $a_{2n}$  (see Fig. 4b,c,d), with a decreasing contribution of mode 0 and an increasing  
 378 contribution of higher and higher  $n$  modes for increasing  $L_y$ . Considering the sensitivity of  
 379 the functions  $\gamma_{2n,i}(L_x)$  to  $n$  explained above, the decrease of  $\Gamma_*$  with  $L_x$  is therefore larger for  
 380 larger  $L_y$ . Since  $\Gamma_*$  is independent of  $L_y$  for  $L_x = 0$ , this explains the sensitivity of  $\Gamma_*$  to both  
 381  $L_x$  and  $L_y$ .

382

383 •  $L_y < 1$ , there is still a strong influence of the response of mode  $n = 0$  and the influence of  
 384 modes with larger  $n$  is complex. For  $L_y$  close to zero, both  $a_{2n}(0)$  and  $I_{2n} \approx 8L_y D_{2n}(0)$  al-  
 385 ternate sign as  $(-1)^n$  (see Eqs. (27) and (A5)), so  $f_{2n}$  is positive for all  $n$ . But  $f_{2n} - g_{2n,1}$   
 386 is negative for  $n > 0$  which means that the contributions to the circulation  $\Gamma_*^{(2n,1)}$  increases  
 387 with increasing  $L_x$ .  $f_{2n} - g_{2n,2}$  is positive and  $\Gamma_*^{(2n,2)}$  decreases with increasing  $L_x$  and com-  
 388 pensates the increase of  $\Gamma_*^{(2n,1)}$ . For  $L_y$  closer to 1,  $f_{2n}$ ,  $g_{2n,1}$ ,  $g_{2n,2}$ , and their differences  
 389 can change sign for  $n > 0$  since  $D_{2n}$  and  $D_{2n\pm 1}$  changes sign at least once over the interval  
 390  $[-4L_y, 4L_y]$ , resulting in an increase of the contributions  $\Gamma_*^{(2n,i)}$  with increasing  $L_x$  in intervals  
 391 where  $a_{2n}(f_{2n} - g_{2n,i}) < 0$ . These contributions in these intervals reduce the sensitivity of  $\Gamma_*$

---

<sup>2</sup> $I_{2n}^\infty = \frac{\sqrt{\pi}(2n)!}{2^{n-1}n!}$

392 to  $L_x$  and, since  $\Gamma_*(0, L_y)$  is a constant,  $\Gamma_*$  for  $L_x \neq 0$  is larger for reduced sensitivity to  $L_x$ ,  
 393 i.e., for smaller  $L_y$ .

394 Despite this overall complexity, it appears clearly that the two components of the response to heat-  
 395 ing along  $D_0$  are the main contributors to  $\Gamma_*$  and its sensitivity. This is because in this mode, the  
 396 Kelvin-wave pattern and the Rossby-wave pattern both contribute to low level wind convergence  
 397 in the region of ascent through the easterlies at the eastern boundary (for the first component) and  
 398 westerlies at the western boundary (for the second component). By contrast, the two components  
 399 for modes with  $n > 0$  are opposite close to the equator, with gyres that circulate in opposite direc-  
 400 tions, and there is a significant amount of compensation between components of the response to  
 401 heating along  $D_{2n}$  with  $n > 0$ .

402 Thanks to the continuity equation, we can also decompose  $\Gamma_*$  into the sum of a contribution  
 403 from the meridional wind ( $v$  integrated over the boundary at  $y = \pm 4L_y$ ) and a contribution  $\Gamma_{*u}$   
 404 from the zonal wind ( $u$  integrated over the boundaries at  $x = \pm L_x$ ). And each contribution  $\Gamma_*^{(2n,i)}$   
 405 can also be decomposed in the same way:

$$\Gamma_* = \Gamma_{*u} + \Gamma_{*v} \quad \text{and} \quad \Gamma_*^{(2n,i)} = \Gamma_{*u}^{(2n,i)} + \Gamma_{*v}^{(2n,i)}$$

406 Because  $u^{(0,1)}(-L_x) = 0$  and  $u^{(2n,i)}(L_x) = 0$  for all  $n > 0$  or  $i = 2$ , the contribution from the zonal  
 407 wind at the eastern border results exclusively from the damped Kelvin wave extending eastward  
 408 from the heating region, while the contribution from the zonal wind at the western border results  
 409 from a combination of damped Rossby waves. By integrating  $u$  given in Equations (21)-(24), we

410 can write (see last paragraph of Appendix B):

$$\Gamma_{*u}^{(2n,1)} = \gamma_{2n}(L_x) [f_{2n}(L_y) - (4n - 1)g_{2n,1}(L_y)], \quad (57)$$

$$\Gamma_{*u}^{(2n,2)} = \gamma_{2n+2}(L_x) [f_{2n}(L_y) + (4n + 3)g_{2n,2}(L_y)], \quad (58)$$

411 and we can compute  $\Gamma_{*u}$  by summing over  $n$ . Figure 3b shows that except for small  $L_y$ ,  $\Gamma_{*u}$  is  
 412 the dominant contribution to  $\Gamma_*$ . The smaller contribution of the meridional wind  $\Gamma_{*v}$  results from  
 413 the partial compensation between the equatorward and poleward branches of the gyres. And the  
 414 westerly low-level zonal flow into the ascending region through its western boundary, which is  
 415 also part of these gyres, contributes very significantly to the overturning circulation. In the limit  
 416  $L_x \rightarrow 0$ ,  $\Gamma_* \approx \Gamma_{*u}$ . Section 2.d also shows that, in this limit,  $w \sim Q$ ; this means that the region of  
 417 ascent is the region of heating which extends to infinity in the latitudinal direction, so that there is  
 418 no flow at the meridional boundaries:

$$\Gamma_u \sim \Gamma \sim [Q] \text{ and } \Gamma_v \sim 0 \quad (59)$$

419 irrespective of  $L_y$ : this result is valid for both  $\Gamma$  and its approximation  $\Gamma_*$ .

420 Figure 3c shows that the contribution  $\Gamma_{*u}^{(0,1)}$  of the damped Kelvin wave represents a significant  
 421 fraction of  $\Gamma_*$  (and  $\Gamma_{*u}$ ) except for small  $L_y$ . This relative contribution is larger than 60% for large  
 422  $L_x$ , which is consistent with the results in Iipponen and Donner (2021, see their Figure 4), and it  
 423 can be as low as one third for small  $L_x$  and large  $L_y$ , which shows the importance of the low-level  
 424 westerly jet associated with the damped Rossby waves for small  $L_x$ , even away from the limit  
 425  $L_y \rightarrow 0$ .

426 *c. Equatorial westerly jet*

427 The main feature of the zonal asymmetry of the Gill circulation is the low-level westerly jet  
428 located at and around the heating center, which does not exist in the  $f$ -plane case. This feature is  
429 of particular interest for the potential coupling of circulation with explicitly modeled diabatic pro-  
430 cesses. Since such a low-level jet can modulate the surface turbulent heat fluxes, it could influence  
431 tropical intraseasonal variability (Sobel et al. 2008, 2010) and contribute to horizontal moisture  
432 advection which is thought to contribute to the eastward propagation of tropical intraseasonal dis-  
433 turbances (Maloney et al. 2010; Leroux et al. 2016). The two cyclonic gyres that extend west of  
434 the heating center on both sides of the equator interact constructively to create this jet. As can be  
435 seen in Figure 1, as the scale of the heating decreases, the gyres become smaller, faster, and closer  
436 to the equator, which accelerates the low-level westerly jet and decreases its latitudinal extent. For  
437 infinitely small heating, the jet is infinitely fast at the equator, as established in Section 2.d.

438 As metrics of this jet, we will study the low-level wind speed at the heating center:  $u_0 = -u(0,0)$   
439 ( $u$  describes the first baroclinic mode, so that low-level winds have the opposite sign), the zonal  
440 extent of the jet  $x_u$  defined as the zonal coordinate at which  $u$  changes sign along the x-axis:  
441  $u(x_u, 0) = 0$ , the meridional extent of the jet  $y_u$  defined as the positive meridional coordinate at  
442 which  $u$  changes sign along the y-axis:  $u(0, y_u) = 0$ , and the integrated intensity of the jet:  $U =$   
443  $-\int_{-y_u}^{y_u} u(0, y) dy$ , which describes the low-level eastward mass transport around the equator. Figure  
444 5 shows the sensitivity of these four metrics as a function of  $L_x$  and  $L_y$ .

445 The low-level equatorial wind  $u_0$  at the heating center decreases with both  $L_x$  and  $L_y$  (see Fig.  
446 5a). It tends towards zero for large  $L_x$  or large  $L_y$ , and towards infinity if both  $L_x$  and  $L_y$  tend  
447 towards zero. We can also decompose  $u_0$  into a sum of contributions from the different modes:

$$u_o = \sum_{n=0}^{\infty} u_o^{(2n)} = \sum_{n=0}^{\infty} \left( u_o^{(2n,1)} + u_o^{(2n,2)} \right), \quad (60)$$

448 with  $u_o^{(2n,1)}$  and  $u_o^{(2n,2)}$  the contributions of the first and second components of the response to  
 449 the projection of the heating latitudinal distribution  $D$  on the  $n^{\text{th}}$  symmetric latitudinal mode  $D_{2n}$ .  
 450 Appendix C shows that there is a significant compensation between  $u_o^{(2n,2)}$  and  $u_o^{(2n,1)}$  for  $n > 0$   
 451 because the two gyres straddling the equator have opposite rotation (cyclonic v.s. anticyclonic) in  
 452 the two components. We can write:

$$u_o^{(2n)} = v_{2n}(L_x) h_{2n}(L_y), \quad (61)$$

453 with the variation in  $L_x$  (respectively,  $L_y$ ) encapsulated in the series of functions  $v_{2n}$  (resp.,  $h_{2n}$ ):

$$\begin{aligned} v_0(L_x) &= -\frac{1}{2} q_0^{(0)}(0) + \frac{3}{2} q_2^{(0)}(0), \\ v_{2n}(L_x) &= -\left(n - \frac{1}{4}\right) \frac{q_{2n}^{(2n)}(0)}{2n-1} + \left(n + \frac{3}{4}\right) q_{2n+2}^{(2n)}(0), \text{ for } n > 0. \end{aligned} \quad (62)$$

454

$$\begin{aligned} h_0(L_y) &= a_0(L_y) D_0(0) = \sqrt{\frac{2}{1+L_y^2}}, \\ h_{2n}(L_y) &= 2a_{2n}(L_y) D_{2n}(0) = \frac{(2n)!}{(2^n n!)^2} \left(\frac{1-L_y^2}{1+L_y^2}\right)^n \sqrt{\frac{8}{1+L_y^2}}, \text{ for } n > 0. \end{aligned} \quad (63)$$

455 Figure 6 shows the functions  $v_{2n}$  and  $h_{2n}$  for  $n \leq 5$ . These show that the response to the forcing  
 456 along  $D_0$  is the largest contribution to  $u_o$  except for  $L_x$  and  $L_y \rightarrow 0$ , but most latitudinal modes do  
 457 contribute to the sensitivity of  $u_o$  to  $L_x$  and  $L_y$ . The functions  $v_{2n}$  include the two compensating  
 458 effects of  $u_o^{(2n,1)}$  and  $u_o^{(2n,2)}$ . As a result of this compensation,  $v_{2n}(0) = 1$  is independent of  $n$ , and

459  $v_{2n}$  decreases towards 0 for  $L_x \rightarrow \infty$ . This decrease is faster for larger  $n$ , similarly to the functions  
 460  $\gamma_{2n}$  which describe the sensitivity of  $\Gamma_*$  to  $L_x$ .

461 The functions  $h_{2n}$  describe the sensitivity of  $u_0^{(2n)}$  to  $L_y$ , which is essentially dominated by the  
 462 sensitivity of  $a_{2n}$  in terms of amplitude (see the similarity between Figs. 4b and 6b), but  $D_{2n}(0)$   
 463 contributes to the sign:  $D_{2n}(0)$ 's sign is given by  $(-1)^n$ , while  $a_{2n}$  is given by  $((1 - L_y^2)/(1 + L_y^2))^n$ ;  
 464 as a result,  $h_{2n}$  is positive for all  $n$  if  $L_y < 1$  and for even  $n$  if  $L_y > 1$ ; it is negative for odd  $n$  if  
 465  $L_y > 1$ . As in the case of  $\Gamma_*$ , we find this distinction between two regimes on each side of  $L_y = 1$ :

- 466 • For  $L_y \leq 1$ , all latitudinal modes interact constructively to strengthen the low-level westerly  
 467 jet. The amplitudes of functions  $h_{2n}$  decrease with  $L_y$ . For all  $n > 0$ ,  $h_{2n}$  and its  $(n - 1)$   
 468 first derivatives are zero at  $L_y = 1$ ;  $h_{2n}$  also slowly decreases with increasing  $n$  for  $L_y = 0$   
 469 ( $h_{2n}(0) = (1 - (2n)^{-1})h_{2n-2}(0)$ ).  $h_0$  is different, first because  $h_0(1) = 1$  (case with  $D = D_0$ ),  
 470 and also because  $h_0(0)$  is not larger than  $h_2(0)$ : this results from the specificity of the  
 471 first component of the response to heating along  $D_0$ , i.e., the damped Kelvin wave, which  
 472 decreases the low-level westerly jet more efficiently than a competing gyre. The decrease  
 473 of all  $h_{2n}$  with  $L_y$  in this regime results from the decrease in the amplitudes of projection  
 474 coefficients  $a_{2n}$  with  $L_y$  (see Fig. 4b), which results directly from the smoother latitudinal  
 475 distribution of heating with larger  $L_y$ . Moreover, the decrease in  $|a_{2n}|$  with  $L_y$  is larger for  
 476 larger  $n$ , so that the relative contribution to  $u_0$  from latitudinal modes with large  $n$  decreases  
 477 with  $L_y$ , which decreases its sensitivity to  $L_x$ .

- 478
- 479 • For  $L_y > 1$ , there is still a strong influence of the response of mode  $n = 0$ , and the influence  
 480 of modes with larger  $n$  is complex. Because  $h_{2n}$  changes sign for each increment in  $n$ , there is  
 481 considerable compensation between the contributions from successive latitudinal modes. For

482 even  $n$ ,  $h_{2n} > 0$  and  $u_0^{(2n)}$  decreases with increasing  $L_x$ ; for odd  $n$ ,  $h_{2n} < 0$  and  $u_0^{(2n)}$  increases  
 483 with increasing  $L_x$  ( $|u_0^{2n}|$  decreases), which reduces the sensitivity of  $u_0$  to  $L_x$ . The sensitivity  
 484 of  $|h_{2n}|$  to  $L_y$  is still controlled by that of  $a_{2n}$ . The projection coefficient  $a_0$  decreases as  
 485  $(1 + L_y^2)^{-1}$ , and, for  $n > 0$ ,  $a_{2n}$  increases from zero for  $L_y = 1$  to a maximum for a value  
 486 of  $L_y$  that increases with  $n$ , because  $D$  projects more and more onto latitudinal modes that  
 487 have significant amplitude further and further away from the equator as  $L_y$  increases. As a  
 488 result, the contribution to  $u_0$  from latitudinal modes with  $n > 0$  comes largely from a subset  
 489 of modes with similar  $n$ , with significant compensation between them, and as a result, its  
 490 sensitivity to  $L_y$  results mostly from the contribution of the latitudinal mode  $n = 0$ . For  
 491  $L_y \rightarrow \infty$ , the contributions of latitudinal modes with larger and larger  $n$  get relatively larger,  
 492 but all projections coefficients  $a_{2n}$  tend rapidly to zero, so that  $u_0$  also tends to zero.

493 Figure 5c shows the eastward longitudinal extent  $x_u$  of the low-level westerly jet normalized  
 494 by  $L_x$ . For small  $L_x$  and  $L_y$ ,  $x_u \sim L_x$ , which means that the westerly jet extends over the whole  
 495 heating region at the equator.  $x_u$  decreases with  $L_y$  and increases significantly less than  $L_x$  if  $L_x$   
 496 is increased. For very large  $L_x$  or  $L_y$ ,  $x_u$  tends towards zero (not shown), which means that the  
 497 zonal flow becomes more symmetrical in longitude with respect to the heating center, with low-  
 498 level westerlies to the west and easterlies to the east. Figure 5d shows, on the other hand, that  
 499 the latitudinal extent  $y_u$  of the low-level westerly jet increases mostly with  $L_y$ . For  $L_x \rightarrow 0$ ,  $y_u$   
 500 scales like  $2L_y$  for  $L_y \rightarrow 0$  and this scaling is approximately valid for larger values of  $L_y$  as long as  
 501  $L_x \rightarrow 0$ : the region of westerlies scales in latitude with the heating region. For  $L_x > 0$ ,  $y_u$  is small  
 502 but non-zero for  $L_y = 0$  and the latitudinal widening of the region of westerlies with increasing  $L_y$   
 503 is less pronounced than for  $L_x \rightarrow 0$ . As a result, while  $y_u$  increases slightly with increasing  $L_x$  for  
 504  $L_y \rightarrow 0$ , it decreases with  $L_x$  for  $L_y > 0.7$ . The sensitivities of  $y_u$  and  $u_0$  help explain that of the

505 intensity  $U$  of the low-level westerly jet shown in Figure 5b: as the velocity  $u_0$  at the center of  
 506 the jet decreases with  $L_y$ , its latitudinal extent  $y_u$  increases, and as a result,  $U$  is not very sensitive  
 507 to  $L_y$ . On the other hand,  $U$  decreases with  $L_x$  because of the dominant influence of  $u_0$ . Using  
 508 Equation (42) in Section 2.d, we can confirm the following scalings in the limit  $L_x, L_y \rightarrow 0$ :

$$u_0 \sim \frac{2}{L_y}, \quad (64)$$

$$x_u \sim L_x, \quad (65)$$

$$y_u \sim 2L_y, \text{ and} \quad (66)$$

$$U \sim 2\sqrt{\pi} \operatorname{erf}(1) + 4e^{-1}. \quad (67)$$

509 Note that the maximum westerly wind is located at the equator, west of the heating center (not  
 510 shown). It is furthest from the heating center, at  $(-L_x, 0)$  for  $L_x \rightarrow 0$  (see Section 2.d).

#### 511 **4. Summary and conclusion**

512 In this article, we explore the scale sensitivity of the equatorial Gill circulation, focusing on  
 513 characteristics of this circulation likely to couple it with the energy cycle: we study the sensitivity  
 514 of the overturning circulation intensity (total upward/downward mass flux), which interacts with  
 515 cloud processes, and the characteristics of the low-level westerly flow, which influences turbulent  
 516 surface heat fluxes. In all our cases, we impose the same horizontally-integrated diabatic heating  
 517 in order to understand how the dynamical response of the atmosphere depends on how spatially  
 518 concentrated this diabatic heating is. In this Part I, we study the case of diabatic heating symmetric  
 519 about the equator (Part II studies asymmetric cases).

520 We find that the intensity of the overturning circulation decreases with both the longitudinal and  
 521 the latitudinal extents of the diabatic heating. Part of this sensitivity can be explained by the dif-

522 fusive effect of vertical energy transport on temperature perturbation; as a result, this perturbation  
523  $T$  is spatially smoother than the diabatic heating  $Q$ . This diffusive effect is less efficient for large  
524 horizontal scales of the heating than small scales, because the anomalies of  $T$  directly forced by  
525  $Q$  are smoother. This also means that the vertical motion is smaller for large scales than for small  
526 ones. This sensitivity is enhanced by the influence of rotation, which causes the rotational part  
527 of the horizontal winds to be larger, as evidenced by the off-equatorial gyres west of the heating  
528 region. Since the imposed diabatic heating powers both the divergent and rotational circulations, a  
529 stronger rotational winds result in weaker divergent winds and a less intense overturning circula-  
530 tion. These results suggest that the coupling of the Gill circulation with the energy and hydrologic  
531 cycle would result in a stronger moisture-convergence feedback for small heating regions than for  
532 large ones.

533 As for the low-level westerly jet in the region of diabatic heating, we find that for most metrics, it  
534 is relatively smaller and weaker for large horizontal scales than for small ones. The velocity at the  
535 center of the jet decreases with increasing scales, the latitudinal and longitudinal extents of the jet  
536 increase with increasing scales, but less than the latitudinal and longitudinal scales of the diabatic  
537 heating. The total zonal mass flux in this jet decreases with the longitudinal scale of the diabatic  
538 heating and its sensitivity to the latitudinal scale is small. Overall these results suggest that, in  
539 the heating region, the coupling with surface turbulent heat fluxes would result in a decrease of  
540 surface fluxes in easterlies and an increase in westerlies via the wind-induced surface heat flux  
541 mechanism. Over most of the tropics where trade winds are dominant, this creates a negative  
542 feedback to a diabatic-heating perturbation. Over the equatorial Indian Ocean where winds are  
543 westerlies, this would create a positive feedback. The amplitude of this feedback would be larger  
544 for small heating regions than for large ones.

545 Whether the amplitude and pattern of these moisture-convergence and surface-flux feedbacks  
546 would allow to sustain or enhance a circulation is beyond the scope of this article since it would  
547 require explicit coupling with the hydrologic and energy cycles; all our results provide insights  
548 into the scale sensitivity of such feedbacks.

549 Our results are significant in general for the steady or slowly evolving tropical circulations,  
550 for which the dynamical response is very similar to the steady response. In particular, they are  
551 relevant for the MJO, the fundamental mechanisms of which are still debated (Yano and Tribbia  
552 2017; Rostami and Zeitlin 2019; Zhang et al. 2020, and references therein). While the dynamical  
553 signature of the MJO resembles the symmetric solution described in G80, its latitudinal scale is  
554 smaller, and the scale sensitivity of the overturning circulation combined with its coupling to the  
555 hydrologic cycle might contribute to explaining the MJO scale selection. Also, the MJO convective  
556 disturbances do grow in the equatorial westerlies of the Indian Ocean, and some studies have  
557 suggested that these background winds are crucial to their development (Sobel et al. 2008, 2010;  
558 Maloney et al. 2010; Leroux et al. 2016), particularly because of wind-induced surface-heat-flux  
559 feedback described above, but also because of horizontal moisture advection; the scale sensitivity  
560 of the low-level westerly jet suggests that such mechanisms are particularly active for perturbations  
561 of small horizontal extent, e.g., during the development of MJO disturbances.

562 The observed MJO and interannual climate variability provide multiple opportunities to evaluate  
563 whether the scale dependency of observed circulations responding to equatorial heating follows  
564 the sensitivity predicted by the Gill circulation. This will be the topic of further work.

565 *Acknowledgments.* The authors thank Jean-Philippe Duvel for his useful comments. The authors  
566 also acknowledge the support of the University of Auckland, and particularly financial support

<sup>567</sup> from its Faculty of Science in the form a PhD fellowship and a grant from the Faculty Research  
<sup>568</sup> Development Fund. G.B. is also supported by the Glavish-Buckley Lectureship.

### A few properties of the parabolic cylinder functions $D_n$

571 The parabolic cylinder functions  $D_n$  are defined by the recursive Equation (7). They also verify,  
572 as pointed out by G80 (their Equations (3.7) and (3.8)):

$$\frac{dD_n}{dy} + \frac{y}{2}D_n = nD_{n-1}, \quad (\text{A1})$$

$$\frac{dD_n}{dy} - \frac{y}{2}D_n = -D_{n+1}, \quad (\text{A2})$$

573 and they are solutions of the differential equations:

$$\frac{d^2D_n}{dy^2} + \left(n + \frac{1}{2} - \frac{y^2}{4}\right)D_n = 0. \quad (\text{A3})$$

574  $D_{2n}$  are even functions and  $D_{2n+1}$  are odd functions of  $y$ . We have:

$$D_{2n+1}(0) = 0 = \frac{dD_{2n}}{dy}(0), \quad (\text{A4})$$

$$D_{2n}(0) = -(2n+1)D_{2n-2}(0) = \left(-\frac{1}{2}\right)^n \frac{(2n)!}{n!} = -\frac{dD_{2n+1}}{dy}(0). \quad (\text{A5})$$

575 Using Equations (A1) and (A2), we can also write:

$$\int_{Y_1}^{Y_2} D_{n+1} dy = n \int_{Y_1}^{Y_2} D_{n-1} dy - 2[D_n(Y_2) - D_n(Y_1)]. \quad (\text{A6})$$

### Contributions of the latitudinal modes to $\Gamma_*$

578 By using the expressions of  $w^{(2n,i)}$  ( $i = 1$  or  $2$ ) in Equation (25) combined with the expressions of  
 579  $T^{(2n,i)}$  from Equations (23) and (24) we can write  $\Gamma_*^{(2n,i)}$  as:

$$\Gamma_*^{(2n,1)} = a_{2n} \left( I_{2n} - \frac{\varepsilon}{2} \int_{-L_x}^{L_x} q_{2n}^{(2n)} dx [I_{2n} + 2nI_{2n-2}] \right), \quad (\text{B1})$$

$$\Gamma_*^{(2n,2)} = a_{2n} \left( I_{2n} - \frac{\varepsilon}{2} \int_{-L_x}^{L_x} q_{2n+2}^{(2n)} dx [I_{2n+2} + (2n+2)I_{2n}] \right), \quad (\text{B2})$$

580 for all  $n$ . We have used  $\int_{-L_x}^{L_x} F dx = 2$  and introduced the notation  $I_{2n} = \int_{-4L_y}^{4L_y} D_{2n} dy$  for  $n \geq 0$  and  
 581  $I_{-2} = 0$ .

582 The differential Equations (11) and (14) yield the following expressions for the integrals of the  
 583 functions  $q_{2n(+2)}^{(2n)}$ :

$$\varepsilon \int_{-L_x}^{L_x} q_0^{(0)} dx = 2 - q_0^{(0)}(L_x), \quad (\text{B3})$$

$$\varepsilon \int_{-L_x}^{L_x} q_{2n}^{(2n)} dx = \frac{1}{4n-1} [4n-2 - q_{2n}^{(2n)}(-L_x)] \quad \text{for } n > 0, \quad (\text{B4})$$

$$\text{and } \varepsilon \int_{-L_x}^{L_x} q_{2n+2}^{(2n)} dx = \frac{1}{4n+3} [2 - q_{2n+2}^{(2n)}(-L_x)] \quad \text{for all } n, \quad (\text{B5})$$

584 in which we have used  $q_0^{(0)}(-L_x) = 0$ ,  $q_{2n}^{(2n)}(L_x) = 0$  for  $n > 0$ , and  $q_{2n+2}^{(2n)}(L_x) = 0$  for all  $n$ .

585 Equation (A6) yields:

$$I_{2n-2} = \frac{1}{2n-1} (I_{2n} + 4D_{2n-1}(4L_y)) \quad \text{and} \quad I_{2n+2} = (2n+1)I_{2n} - 4D_{2n+1}(4L_y). \quad (\text{B6})$$

586 Using Equations (B3)-(B6), Equations (B1) and (B2) can be rewritten:

$$\Gamma_*^{(0,1)} = \frac{q_0^{(0)}(L_x)}{2} a_0 I_0, \quad (\text{B7})$$

$$\Gamma_*^{(2n,1)} = \frac{q_{2n}^{(2n)}(-L_x)}{4n-2} a_{2n} I_{2n} - \frac{8n}{4n-1} a_{2n} D_{2n-1}(4L_y) \left(1 - \frac{q_{2n}^{(2n)}(-L_x)}{4n-2}\right) \text{ for } n > 0, \quad (\text{B8})$$

$$\Gamma_*^{(2n,2)} = \frac{q_{2n+2}^{(2n)}(-L_x)}{2} a_{2n} I_{2n} + \frac{4}{4n+3} a_{2n} D_{2n+1}(4L_y) \left(1 - \frac{q_{2n+2}^{(2n)}(-L_x)}{2}\right) \text{ for all } n. \quad (\text{B9})$$

587 By replacing  $q_{2n}^{(2n)}$  by its expression from Equations (17) and (19), and using  $q_{2n}^{(2n)} =$   
 588  $(2n-1)q_{2n}^{(2n-2)}$ ,  $\Gamma_*^{(2n,i)}$  can be written as in Equations (50) and (51).

589

590 The contribution  $\Gamma_{*u}^{(2n,i)}$  to  $\Gamma_*^{(2n,i)}$  from the zonal flow is simply the integral of the zonal velocity  
 591  $u^{(2n,i)}$  over the zonal boundary of the the rectangle  $(2L_x, 8L_y)$  where it is not zero, multiplied by  
 592  $\pm a_{2n}$ . Using Equations (21), (23), and (24), it can be written as:

$$\Gamma_{*u}^{(0,1)} = \frac{a_0}{2} q_0^{(0)}(L_x) I_0 = \Gamma_*^{(0,1)}, \quad (\text{B10})$$

$$\Gamma_{*u}^{(2n,1)} = -\frac{a_{2n}}{2} q_{2n}^{(2n)}(-L_x) [I_{2n} - 2n I_{2n-2}] \text{ for } n > 0, \quad (\text{B11})$$

$$\Gamma_{*u}^{(2n,2)} = -\frac{a_{2n}}{2} q_{2n+2}^{(2n)}(-L_x) [I_{2n+2} - (2n+2) I_{2n}] \text{ for all } n. \quad (\text{B12})$$

593 The last two can be simplified using Equation (B6) into:

$$\Gamma_{*u}^{(2n,1)} = \frac{q_{2n}^{(2n)}(-L_x)}{4n-2} a_{2n} [I_{2n} + 8n D_{2n-1}(4L_y)] \text{ for } n > 0, \quad (\text{B13})$$

$$\Gamma_{*u}^{(2n,2)} = \frac{q_{2n+2}^{(2n)}(-L_x)}{2} a_{2n} [I_{2n} + 4D_{2n+1}(4L_y)] \text{ for all } n. \quad (\text{B14})$$

594 By replacing  $q_{2n}^{(2n)}$  by its expression from Equations (17) and (19), and using  $q_{2n}^{(2n)} = (2n -$   
 595  $1)q_{2n}^{(2n-2)}$ ,  $\Gamma_{*u}^{(2n,i)}$  can be written as in Equations (57) and (58).

## 596 APPENDIX C

### 597 Contributions of the latitudinal modes to $u_0$

598 By using the expressions of  $u^{(2n,i)}$  ( $i = 1$  or  $2$ ) in Equations (23) and (24) we can write  $u_0^{(2n,i)}$  as:

$$u_0^{(0,1)} = -\frac{a_0}{2}q_0^{(0)}(0)D_0(0), \quad (\text{C1})$$

$$u_0^{(2n,1)} = -\frac{a_{2n}}{2}q_{2n}^{(2n)}(0)[D_{2n}(0) - 2nD_{2n-2}(0)] \text{ for } n > 0, \quad (\text{C2})$$

$$u_0^{(2n,2)} = -\frac{a_{2n}}{2}q_{2n+2}^{(2n)}(0)[D_{2n+2}(0) - (2n+2)D_{2n}(0)] \text{ for all } n \quad (\text{C3})$$

599 Using Equation (A5), we can express the linear combinations of latitudinal modes at  $y = 0$  as  
 600 proportional to  $D_{2n}(0)$ :

$$u_0^{(2n,1)} = -\frac{a_{2n}}{2}q_{2n}^{(2n)}(0)\frac{4n-1}{2n-1}D_{2n}(0), \quad (\text{C4})$$

$$u_0^{(2n,2)} = \frac{a_{2n}}{2}q_{2n+2}^{(2n)}(0)(4n+3)D_{2n}(0), \quad (\text{C5})$$

601 for all  $n$ .  $u^{(0,1)}$  is the westward wind associated with the Kelvin-wave response.  $u_0^{(2n,1)}$  is the  
 602 westward equatorial branch of the anticyclonic gyres along the equator for  $n > 0$  and  $u_0^{(2n,2)}$  is  
 603 the eastward equatorial branch of the cyclonic gyres along the equator. They both scale with  $n$   
 604 and there is considerable compensation between them; therefore it does not provide any insight to  
 605 present them independently. Their sum yields Equation (61).

606 **References**

- 607 Abramowitz, M., and I. A. Stegun, 1964: *Handbook of Mathematical Functions with Formulas,*  
608 *Graphs, and Mathematical Tables.* ninth dove ed., Dover, New York.
- 609 Adam, O., 2018: Zonally Varying ITCZs in a Matsuno-Gill-Type Model With an Idealized  
610 Bjerknes Feedback. *Journal of Advances in Modeling Earth Systems*, **10** (6), 1304–1318, doi:  
611 10.1029/2017MS001183.
- 612 Back, L. E., and C. S. Bretherton, 2009: On the relationship between sst gradients, boundary  
613 layer winds, and convergence over the tropical oceans. *Journal of Climate*, **22** (15), 4182–4196,  
614 doi:10.1175/2009JCLI2392.1.
- 615 Battisti, D. S., E. S. Sarachik, and A. C. Hirst, 1999: A Consistent Model for the Large-Scale  
616 Steady Surface Atmospheric Circulation in the Tropics\*. *Journal of Climate*, **12** (10), 2956–  
617 2964, doi:10.1175/1520-0442(1999)012<2956:ACMFTL>2.0.CO;2.
- 618 Bellon, G., and B. Reboredo, 2021: Scale sensitivity of the Gill circulation, Part II: off-equatorial  
619 case. *Journal of the Atmospheric Sciences*, submitted.
- 620 Bretherton, C. S., and A. H. Sobel, 2003: The Gill Model and the Weak Temperature Gra-  
621 dient Approximation. *Journal of the Atmospheric Sciences*, **60** (2), 451–460, doi:10.1175/  
622 1520-0469(2003)060<0451:TGMATW>2.0.CO;2.
- 623 Cauchy, A. L. B., 1821: *Cours d'analyse de l'École Royale Polytechnique: Analyse algébrique.*  
624 *I.re partie.* Debure frères, Paris.
- 625 Gill, A. E., 1980: Some simple solutions for heat-induced tropical circulation. *Quarterly Journal*  
626 *of the Royal Meteorological Society*, **106** (449), 447–462, doi:10.1002/qj.49710644905.

627 Heckley, W. A., and A. E. Gill, 1984: Some simple analytical solutions to the problem of forced  
628 equatorial long waves. *Quarterly Journal of the Royal Meteorological Society*, **110** (463), 203–  
629 217, doi:10.1002/qj.49711046314.

630 Hendon, H. H., and M. L. Salby, 1994: The Life Cycle of the Madden–Julian Oscillation. *Jour-  
631 nal of the Atmospheric Sciences*, **51** (15), 2225–2237, doi:10.1175/1520-0469(1994)051<2225:  
632 TLCOTM>2.0.CO;2.

633 Iipponen, J., and L. Donner, 2021: Simple analytic solutions for a convectively driven walker  
634 circulation and their relevance to observations. *Journal of the Atmospheric Sciences*, **78** (1), 299  
635 – 311, doi:10.1175/JAS-D-20-0014.1, URL [https://journals.ametsoc.org/view/journals/atsc/78/  
636 1/jas-d-20-0014.1.xml](https://journals.ametsoc.org/view/journals/atsc/78/1/jas-d-20-0014.1.xml).

637 Kiladis, G. N., K. H. Straub, and P. T. Haertel, 2005: Zonal and Vertical Structure of the  
638 Madden–Julian Oscillation. *Journal of the Atmospheric Sciences*, **62** (8), 2790–2809, doi:  
639 10.1175/JAS3520.1.

640 Krueger, A. F., and J. S. Winston, 1974: A Comparison of the Flow Over the Tropics During  
641 Two Contrasting Circulation Regimes. *Journal of the Atmospheric Sciences*, **31** (2), 358–370,  
642 doi:10.1175/1520-0469(1974)031<0358:ACOTFO>2.0.CO;2.

643 Leroux, S., and Coauthors, 2016: Inter-model comparison of subseasonal tropical variability in  
644 aquaplanet experiments: Effect of a warm pool. *Journal of Advances in Modeling Earth Sys-  
645 tems*, **8** (4), 1526–1551, doi:10.1002/2016MS000683.

646 Lin, J.-L., B. E. Mapes, and W. Han, 2008: What Are the Sources of Mechanical Damping in  
647 Matsuno–Gill-Type Models? *Journal of Climate*, **21** (2), 165–179, doi:10.1175/2007JCLI1546.  
648 1.

- 649 Lin, J.-L., M. Zhang, and B. Mapes, 2005: Zonal Momentum Budget of the Madden–Julian Os-  
650 cillation: The Source and Strength of Equivalent Linear Damping. *Journal of the Atmospheric*  
651 *Sciences*, **62** (7), 2172–2188, doi:10.1175/jas3471.1.
- 652 Lintner, B. R., G. Bellon, A. H. Sobel, D. Kim, and J. D. Neelin, 2012: Implementation of the  
653 Quasi-equilibrium Tropical Circulation Model 2 (QTCM2): Global simulations and convection  
654 sensitivity to free tropospheric moisture. *Journal of Advances in Modeling Earth Systems*, **4**,  
655 M12 002, doi:10.1029/2012MS000174.
- 656 Madden, R. A., and P. R. Julian, 1971: Detection of a 40–50 Day Oscillation in the Zonal Wind  
657 in the Tropical Pacific. *Journal of the Atmospheric Sciences*, **28** (5), 702–708, doi:10.1175/  
658 1520-0469(1971)028<0702:DOADOI>2.0.CO;2.
- 659 Maloney, E. D., A. H. Sobel, and W. M. Hannah, 2010: Intraseasonal variability in an aquaplanet  
660 general circulation model. *Journal of Advances in Modeling Earth Systems*, **2**, 5, doi:10.3894/  
661 JAMES.2010.2.5.
- 662 Matsuno, T., 1966: Quasi-geostrophic motions in the equatorial area. *Journal of the Meteorologi-*  
663 *cal Society of Japan*, **44** (February), 25–43, doi:10.1002/qj.49710644905.
- 664 Neelin, J. D., 1989: On the interpretation of the Gill model. *Journal of the Atmospheric Sciences*,  
665 **46** (15), 2466–2468, doi:10.1175/1520-0469(1989)046<2466:OTIOTG>2.0.CO;2.
- 666 Neelin, J. D., and N. Zeng, 2000: A Quasi-Equilibrium Tropical Circulation  
667 Model—Formulation\*. *Journal of the Atmospheric Sciences*, **57** (11), 1741–1766, doi:  
668 10.1175/1520-0469(2000)057<1741:AQETCM>2.0.CO;2.

669 Pazan, S. E., and G. Meyers, 1982: Interannual Fluctuations of the Tropical Pacific Wind  
670 Field and the Southern Oscillation. *Monthly Weather Review*, **110** (6), 587–600, doi:10.1175/  
671 1520-0493(1982)110(0587:IFOTTP)2.0.CO;2.

672 Philander, S. G. H., 1983: El Niño Southern Oscillation phenomena. *Nature*, **302** (5906), 295–301,  
673 doi:10.1038/302295a0.

674 Pierrehumbert, R. T., and M. Hammond, 2019: Atmospheric circulation of tide-locked exoplanets.  
675 *Annual Review of Fluid Mechanics*, **51**, 275–303, doi:10.1146/annurev-fluid-010518-040516.

676 Rostami, M., and V. Zeitlin, 2019: Eastward-moving convection-enhanced modons in shallow  
677 water in the equatorial tangent plane. *Physics of Fluids*, **31** (2), 021 701, doi:10.1063/1.5080415.

678 Showman, A. P., and L. M. Polvani, 2010: The Matsuno-Gill model and equatorial superrotation.  
679 *Geophysical Research Letters*, **37** (18), doi:10.1029/2010gl044343.

680 Showman, A. P., and L. M. Polvani, 2011: Equatorial superrotation on tidally locked exoplanets.  
681 *The Astrophysical Journal*, **738** (1), 71, doi:10.1088/0004-637x/738/1/71.

682 Sobel, A. H., and C. S. Bretherton, 2000: Modeling tropical precipitation in a single column.  
683 *Journal of Climate*, **13**, 4378–4392, doi:10.1175/1520-0442(2000)013(4378:MTPIAS)2.0.CO;  
684 2.

685 Sobel, A. H., E. D. Maloney, G. Bellon, and D. M. Frierson, 2008: The role of surface heat fluxes in  
686 tropical intraseasonal oscillations. *Nature Geoscience*, **1** (10), 653–657, doi:10.1038/ngeo312.

687 Sobel, A. H., E. D. Maloney, G. Bellon, and D. M. Frierson, 2010: Surface fluxes and tropical  
688 intraseasonal variability: A reassessment. *Journal of Advances in Modeling Earth Systems*, **2**,  
689 1–27, doi:10.3894/JAMES.2010.2.2.

- 690 Stechmann, S. N., and H. R. Ogrosky, 2014: The Walker circulation, diabatic heating, and out-  
691 going longwave radiation. *Geophysical Research Letters*, **41** (24), 9097–9105, doi:10.1002/  
692 2014GL062257.
- 693 Yano, J.-I., and J. J. Tribbia, 2017: Tropical Atmospheric Madden–Julian Oscillation: A Strongly  
694 Nonlinear Free Solitary Rossby Wave? *Journal of the Atmospheric Sciences*, **74** (10), 3473–  
695 3489, doi:10.1175/jas-d-16-0319.1.
- 696 Yu, J.-Y., C. Chou, and J. D. Neelin, 1998: Estimating the gross moist stability of the tropical atmo-  
697 sphere. *Journal of the atmospheric sciences*, **55** (8), 1354–1372, doi:10.1175/1520-0469(1998)  
698 055<1354:etgmso>2.0.co;2.
- 699 Zeng, N., J. D. Neelin, and C. Chou, 2000: A Quasi-Equilibrium Tropical Circulation  
700 Model—Implementation and Simulation\*. *Journal of the Atmospheric Sciences*, **57** (11), 1767–  
701 1796, doi:10.1175/1520-0469(2000)057<1767:AQETCM>2.0.CO;2.
- 702 Zhang, C., 2005: Madden-Julian Oscillation. *Reviews of Geophysics*, **43** (2), RG2003, doi:10.  
703 1029/2004RG000158.
- 704 Zhang, C., Á. Adames, B. Khouider, B. Wang, and D. Yang, 2020: Four theories of the Madden-  
705 Julian Oscillation. *Reviews of Geophysics*, **58** (3), doi:10.1029/2019rg000685.
- 706 Zhang, Z., and T. N. Krishnamurti, 1996: A Generalization of Gill’s Heat-Induced Tropical Circu-  
707 lation. *Journal of the Atmospheric Sciences*, **53** (7), 1045–1052, doi:10.1175/1520-0469(1996)  
708 053<1045:AGOGHI>2.0.CO;2.

709 **LIST OF FIGURES**

710 **Fig. 1.** Solutions for the Gill circulation: temperature response (contours) and low-level velocity  
711 (vectors) for (a)  $L_y = 1$  (equatorial radius of deformation), (b)  $L_y = 1/2$ , and (c)  $L_y = 1/4$ .  
712 In all cases,  $L_x = 3L_y$ . . . . . 46

713 **Fig. 2.** Forcing and solution for the Gill circulation: heating (dashed lines) and mid-tropospheric  
714 vertical velocity (solid lines) for (a)  $L_y = 1$ , (b)  $L_y = 1/2$ , and (c)  $L_y = 1/4$ . In all cases,  
715  $L_x = 3L_y$ . . . . . 47

716 **Fig. 3.** (a) Intensity  $\Gamma$  of the overturning circulation; the letters "a", "b", and "c" indicate the cases  
717 shown in Figures 1 and 2, and "G80" indicates the case discussed in G80 (contours interval  
718 0.5); (b) Contribution  $\Gamma_{*u}$  of the zonal flow to the overturning circulation (in % of  $\Gamma_*$ ); and  
719 (c) Contribution  $\Gamma_{*u}^{(0,1)}$  of the easterly flow to the overturning circulation (in % of  $\Gamma_*$ ). . . . . 48

720 **Fig. 4.** Functions determining the sensitivity of the contribution  $\Gamma_*^{(2n,i)}$  to the longitudinal extent  $L_x$   
721 and  $L_y$  of heating for  $n \leq 5$ : (a)  $\gamma_{2n}(L_x)$  gives the variation of  $\Gamma_*^{(2n,1)}$  and  $\Gamma_*^{(2n-2,2)}$  from the  
722  $f_{2n}$  for  $L_x = 0$  to, respectively,  $g_{2n,1}$  and  $g_{2n,2}$  for  $L_x \rightarrow \infty$ ; (b)  $a_{2n}$  the projection coefficient of  
723  $D$  on the latitudinal mode  $D_{2n}$ , normalized by  $|a_{2n}(0)/a_0(0)|$ ; (c)  $f_{2n}$  (thick lines) and  $g_{2n,1}$   
724 (thin lines) give the limits of  $\Gamma_*^{(2n,1)}$  for, respectively,  $L_x = 0$  and  $L_x \rightarrow \infty$ ; and (d)  $f_{2n}$  (thick  
725 lines) and  $g_{2n,2}$  (thin lines) give the limits of  $\Gamma_*^{(2n,2)}$  for, respectively,  $L_x = 0$  and  $L_x \rightarrow \infty$ . . . . . 49

726 **Fig. 5.** Characteristics of the equatorial westerly jet in the Gill circulation: (a) westerly zonal ve-  
727 locity at the origin  $u_0$ ; the letters "a", "b", and "c" indicate the cases shown in Figures 1 and  
728 2 and "G80" indicates the case discussed in G80; (b) Intensity  $U$  of the jet; (c) Zonal extent  
729  $x_u$  of the jet normalized by  $L_x$ ; (d) meridional extent  $y_u$  of the jet. . . . . 50

730 **Fig. 6.** Functions determining the sensitivity of the contributions  $u_0^{(2n)}$  to the westerly zonal velocity  
731 at the origin  $u_0$  for  $n \leq 5$ : (a)  $v_{2n}(L_x)$  gives the variation of  $u_0^{(2n)}$  with  $L_x$  and (b)  $h_{2n}$  gives  
732 the variation of  $u_0^{(2n)}$  with  $L_y$ . . . . . 51

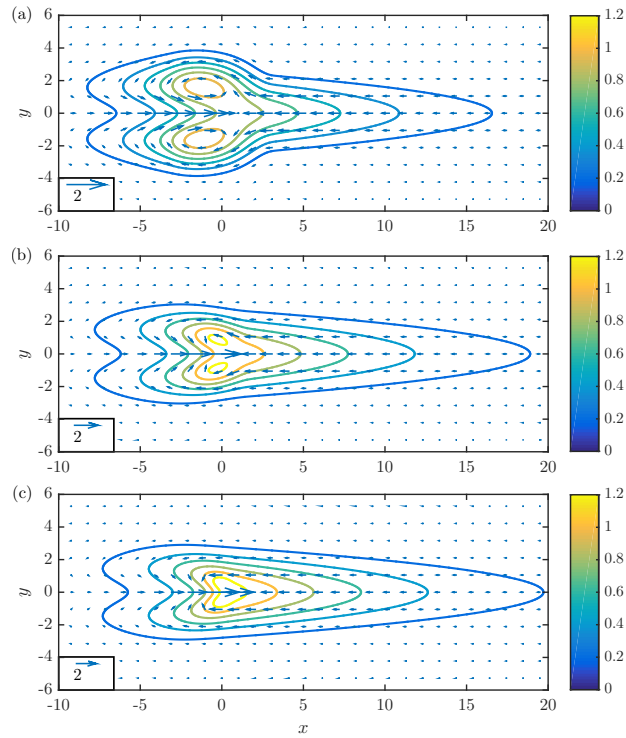


FIG. 1: Solutions for the Gill circulation: temperature response (contours) and low-level velocity (vectors) for (a)  $L_y = 1$  (equatorial radius of deformation), (b)  $L_y = 1/2$ , and (c)  $L_y = 1/4$ . In all cases,  $L_x = 3L_y$ .

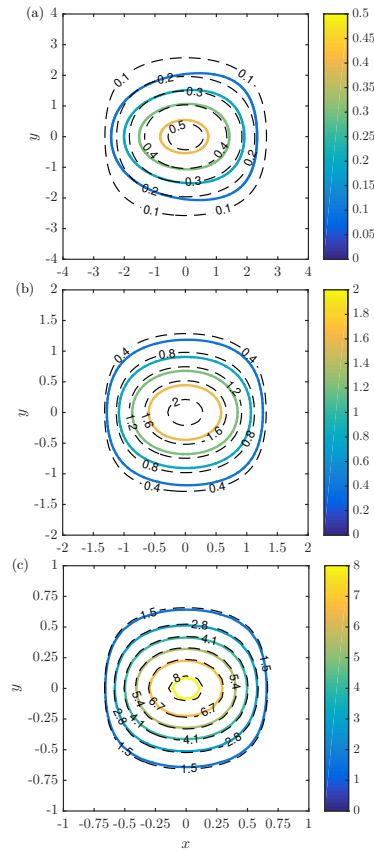


FIG. 2: Forcing and solution for the Gill circulation: heating (dashed lines) and mid-tropospheric vertical velocity (solid lines) for (a)  $L_y = 1$ , (b)  $L_y = 1/2$ , and (c)  $L_y = 1/4$ . In all cases,  $L_x = 3L_y$ .

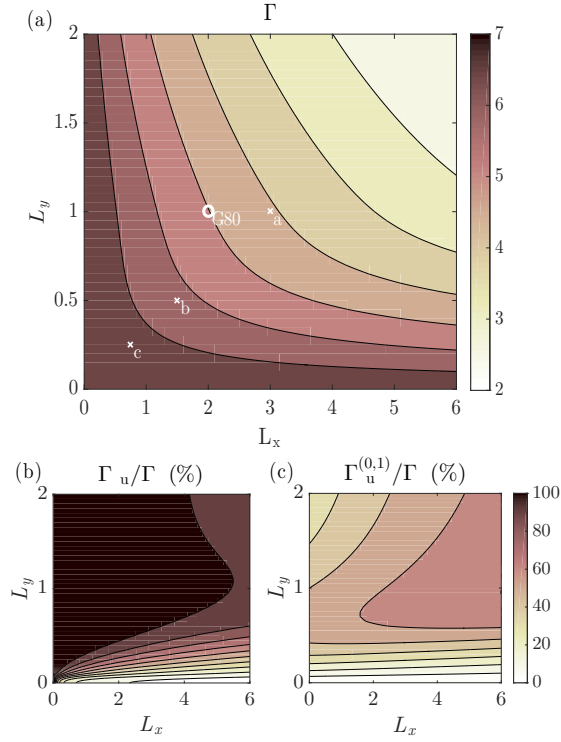


FIG. 3: (a) Intensity  $\Gamma$  of the overturning circulation; the letters "a", "b", and "c" indicate the cases shown in Figures 1 and 2, and "G80" indicates the case discussed in G80 (contours interval 0.5); (b) Contribution  $\Gamma_{*u}$  of the zonal flow to the overturning circulation (in % of  $\Gamma_*$ ); and (c) Contribution  $\Gamma_{*u}^{(0,1)}$  of the easterly flow to the overturning circulation (in % of  $\Gamma_*$ ).

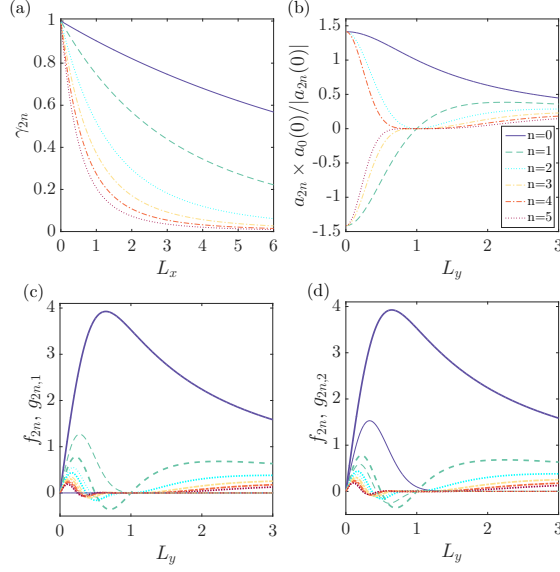


FIG. 4: Functions determining the sensitivity of the contribution  $\Gamma_*^{(2n,i)}$  to the longitudinal extent  $L_x$  and  $L_y$  of heating for  $n \leq 5$ : (a)  $\gamma_{2n}(L_x)$  gives the variation of  $\Gamma_*^{(2n,1)}$  and  $\Gamma_*^{(2n-2,2)}$  from the  $f_{2n}$  for  $L_x = 0$  to, respectively,  $g_{2n,1}$  and  $g_{2n,2}$  for  $L_x \rightarrow \infty$ ; (b)  $a_{2n}$  the projection coefficient of  $D$  on the latitudinal mode  $D_{2n}$ , normalized by  $|a_{2n}(0)/a_0(0)|$ ; (c)  $f_{2n}$  (thick lines) and  $g_{2n,1}$  (thin lines) give the limits of  $\Gamma_*^{(2n,1)}$  for, respectively,  $L_x = 0$  and  $L_x \rightarrow \infty$ ; and (d)  $f_{2n}$  (thick lines) and  $g_{2n,2}$  (thin lines) give the limits of  $\Gamma_*^{(2n,2)}$  for, respectively,  $L_x = 0$  and  $L_x \rightarrow \infty$ .

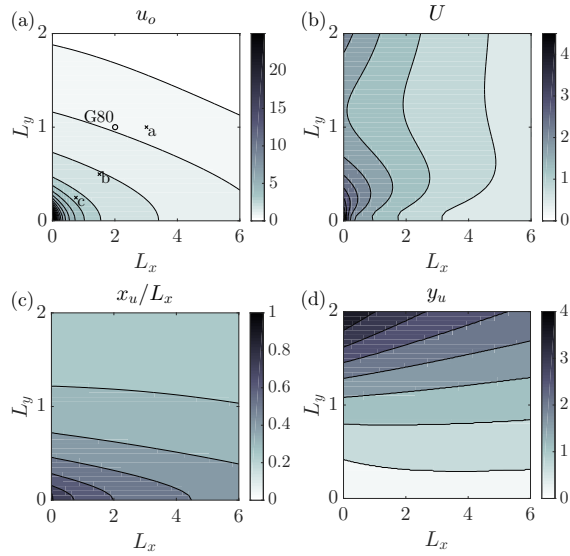


FIG. 5: Characteristics of the equatorial westerly jet in the Gill circulation: (a) westerly zonal velocity at the origin  $u_o$ ; the letters "a", "b", and "c" indicate the cases shown in Figures 1 and 2 and "G80" indicates the case discussed in G80; (b) Intensity  $U$  of the jet; (c) Zonal extent  $x_u$  of the jet normalized by  $L_x$ ; (d) meridional extent  $y_u$  of the jet.

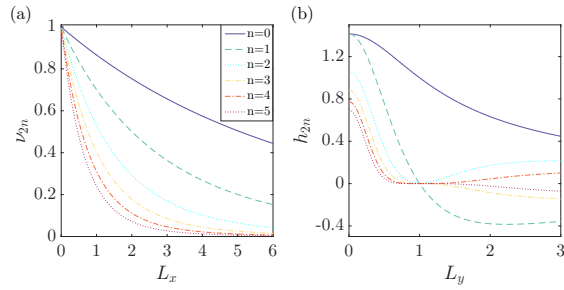


FIG. 6: Functions determining the sensitivity of the contributions  $u_0^{(2n)}$  to the westerly zonal velocity at the origin  $u_0$  for  $n \leq 5$ : (a)  $v_{2n}(L_x)$  gives the variation of  $u_0^{(2n)}$  with  $L_x$  and (b)  $h_{2n}$  gives the variation of  $u_0^{(2n)}$  with  $L_y$ .